Online Data Supplement

GPR183 antagonism reduces macrophage infiltration in influenza and SARS-CoV-2 infection

Cheng Xiang Foo[1#], Stacey Bartlett[1#], Keng Yih Chew[2,] Minh Dao Ngo[1], Helle Bielefeldt-Ohmann[2,3], Buddhika Jayakody Arachchige[4], Benjamin Matthews[4], Sarah Reed[4], Ran Wang[1], Christian Smith[1], Matthew J. Sweet[3,5], Lucy Burr[6], Kavita Bisht[1], Svetlana Shatunova[1], Jane E. Sinclair[2], Rhys Parry[2], Yuanhao Yang[1], Jean-Pierre Lévesque[1], Alexander Khromykh[2,3], Mette Marie Rosenkilde[7], Kirsty R. Short[2,3], and Katharina Ronacher[1,3*]

Methods

Mouse models

IAV infected mice were sacrificed at 3 dpi and 7 dpi for examination. SARS-CoV-2 infected mice were sacrificed at 2 dpi and 5 dpi. Lungs were homogenised in DMEM for use in plaque assays and ELISAs. For RNA processing, lungs were collected in TRIzol (Invitrogen). For oxysterol extractions, lungs and BAL fluid were collected in methanol. For histological analysis the lungs were fixed in 10% neutral buffered formalin.

Mouse-adapted SARS-CoV-2 strain

Six x 10^4 PFU of B1.351 was administrated intranasally to ketamine-anesthetized mice. Mice were monitored daily for weight loss and clinical signs of disease severity. Four days after inoculation, mice were euthanised, and bronchoalveolar lavage (BAL)

was performed. The bronchoalveolar lavage fluid (BALF) was subsequently pooled and used to intranasally inoculate a new batch of mice. The process was repeated until a virulent phenotype of the virus was observed as determined by weight loss and clinical signs, which happened after four passages. To determine whether the mouse adapted SARS-CoV-2 acquired mutations sequencing of viral RNA was performed. Briefly, viral RNA was extracted from BALF using the Qiagen Mini kit and the quality confirmed suing the Agilent Bioanalyzer with 210 Expert software. Library preparations were performed using the Illumina Stranded Total RNA Ribo Zero Plus kit. Sequencing was performed using the NextSeq Midoutput kit, 125bp paired-end configuration with 19-25 million reads per sample. Sequencing analysis was executed using Galaxy software. Whole-genome sequencing revealed a C to T mutation in position 10804 of the SARS-CoV-2 Beta genome resulting in the NSP5 mutation P252L. This mutation was rapidly selected from 3.4% in the initial virus stock to 8.8% in passage one. From passage two, this mutation reached consensus (60%) and underwent further fixation in passage three at 87% to final frequency of 92% in passage four. A mutation in NSP5 was detected in this mouse adapted SARS-CoV-2 strain (Figure S1).

BALF of the mice from the fourth passage was subsequently pooled and used to inoculate Vero E6 cells for propagation, creating the viral stocks for our mouse-adapted strain. To verify the virulent phenotype of the mouse-adapted virus was retained after propagation in Vero E6 cells, the cell grown virus was used to inoculate a new batch of mice. The same viral stock was used to infect mice with $8x10^4$ PFU for the experiments described.

Bioinformatic analysis of mouse-adapted SARS-CoV-2 sequence data

Base-called fastq files were mapped to the QLD1520 SARS-CoV-2 isolate (GISAID accession EPI_ISL_968081) using Bowtie2 (v2.4.2) [1] under default alignment conditions. Sub consensus variants of alignment files were identified using iVar (v1.2.2) [2] with a minimum quality score threshold of 20 and depth of 5000. Coverage of mapped alignment files was determined using samtools (v1.3) depth. Frequencies and coverage of variant positions were manually validated using Integrative Genomics Viewer (Version: 2.7.0) [3]. Variant frequencies and alignment depth was visualised using GraphPad Prism (v9.3.1). Raw fastq data generated in this study have been deposited in the Sequence Read Archive hosted by the National Center for Biotechnology Information with accession number PRJNA849351.

BALF collection

Mice were euthanised before performing the BAL procedure. A lavage was performed by injection of 750 µL of PBS supplemented with 2mM EDTA 2mM and 0.5% FBS into the trachea through a cannula. The BAL fluid was subsequently recovered from the lungs and the recovered volume recorded. The BALF was centrifuged at 400 g for 5 minutes. The supernatant was collected and stored in methanol at −80°C for oxysterol extractions. To the cell pellet, 500uL of TRIZol reagent was added for RNA extraction.

Plaque assays

IAV plaque assays were carried out on confluent monolayers of MDCK cells as previously described [4]. SARS-CoV-2 plaque assays were carried out on Vero E6 cells as described previously [5].

Oxysterol extraction from lung tissues and BAL fluid

Lung lobes from IAV and SARS-CoV-2-infected mice were homogenised in methanol. 500 µL of methanol was added to BAL fluid from IAV and SARS-CoV-2-infected mice. Oxysterols were extracted using a 1:1 dichloromethane:methanol solution containing 50 µg/mL BHT in a 30°C ultrasonic bath. Tubes were flushed with nitrogen to displace oxygen, sealed with a polytetrafluoroethylene (PTFE)-lined screw cap, and incubated at 30°C in the ultrasonic bath for 10 mins. Following centrifugation (3,500 rpm, 5 min, 25°C), the supernatant from each sample was decanted into a new tube. For liquid-liquid extraction, Dulbecco's phosphate-buffered saline (DPBS) was added to the supernatant, agitated, and centrifuged at 3,500 rpm for 5 mins at 25°C. The organic layer was recovered and evaporated under nitrogen using a 27-port drying manifold (Pierce; Fisher Scientific, Fair Lawn, NJ). Oxysterols were isolated by solid-phase extraction (SPE) using 200 mg, 3 mL aminopropyl SPE columns (Biotage; Charlotte, NC). The samples were dissolved in 1 ml of hexane and transferred to the SPE column, followed by a rinse with 1 ml of hexane to elute nonpolar compounds. Oxysterols were eluted from the column with 4.5 ml of a 23:1 mixture of chloroform: methanol and dried under nitrogen. Samples were resuspended in 50µl of warm (37°C) 90% methanol with 0.1% DMSO, and placed in an ultrasonic bath for 5 min at 30°C. A standard curve was extracted for 25-OHC (Sigma-Aldrich, H1015) and 7α,25-OHC (SML0541, Sigma-Aldrich) using the above method. Dichloromethane, butylated hydroxytoluene (BHT) and hexane were purchased from Sigma-Aldrich.

Mass spectrometric quantitation of 25-OHC and 7α,25-OHC in lung homogenates

Samples were analysed on an AB Sciex QTRAP® 5500 (ABSCIEX, Redwood City, CA) mass spectrometer coupled to a Shimadzu Nexera2 UHPLC. A Kinetex Pentafluorophenyl (PFP) column (100 × 2.1mm, 1.7µM, 1000A, Phenomenex) was used for the separation of 25-OHC and 7α,25-OHC from other oxysterols. Mobile

phase used for separation were, A - 0.1% formic acid with water and B - 100% acetonitrile with 0.1% formic acid. Five µL of sample were loaded at 0.5 mL/min and separated using linear gradient with increasing percentage of acetonitrile. Samples were washed for 1.3 min after loading with 30% mobile phase B followed by linear gradient of 30% - 70% over 9 min and 70% to 99% over 1 min. The column was washed with 99% mobile phase B for 2 min followed by equilibration with 30% B 2 min before next injection. Column oven and auto-sampler were operated at 50°C and 15°C, respectively. Elution of analytes from the column was monitored in positive ion mode (ESI) with multiple reaction monitoring on ABSciex QTRAP® mass spectrometer equipped with Turbo spray ion source, which was operated at temp 550°C, ion spray voltage of 5500 V, curtain gas (CUR) of 30 psi, ion source gas1 (GS1) of 65 psi and ion source gas 2 (GS2) of 50 psi. Quadrupole 1 and 3 were operated at unit mass resolution at all time during the experiment. MRM pairs 385.3 > 367.3, 385 >133, 385.3 > 147.1 were monitored for 25-OHC and for 7α,25-OHC following MRM pairs were used 383.2 > 365.3, 383.2 > 147.3, 383.2 > 159.0. Deuterated 25-OHC (11099, Sapphire Bioscience, Redfern, Australia) and 7α,25-OHC (700078P, Merck) were used as internal standards. Following MRM transitions were recoded for internal standards 391.1 > 373.2, 391.1 >133.1, 391.1>123.1 (25-OHC) and 407.2 > 389.0 (7α,25-OHC). De-clustering potential (DP), collision energy (CE), entrance (EP) and collision cell exit potential (CXP) were optimised for each MRM pair to maximise the sensitivity. Data was processed using AbSciex MultiQuant™ software (Version 3.0.3). Oxysterol concentrations were subsequently normalised to the lung weights. High-performance liquid chromatography (HPLC) grade methanol, acetonitrile and chloroform were purchased from Merck.

Flow cytometry

Lung lobes of IAV-infected mice were digested in digestion buffer (Librase; Roche) and passed through 40-µm nylon mesh to obtain single cell suspensions. Red blood cell lysis was performed using BD Pharm Lyse (BD Biosciences, San Jose, CA). Cells were stained with Zombie Green Fixable Viability kit (423111, Biolegend) for 20 mins in PBS first, then stained with fluorescence-conjugated antibodies in FACS buffer for 30 mins on ice before flow cytometric analysis on the BD LSRFortessa X20. The following anti-mouse antibodies were used: Zombie Green Fixable Viability kit (423111, Biolegend), PerCP-CD45 (30-F11), Brilliant Ultraviolet 395-CD3e (145-2C11, BD Biosciences), Brilliant Violet (BV) 786-CD4 (L3T4, BD Biosciences), PE/Cyanine7-CD11b (M1/70), BV510-CD11c (N418), APC/Cyanine7-F4/80 (BM8), BV605-Ly6G (1A8, BD Bioscience), PE-B220 (RA3-6B2), BV421-I-A/I-E (M5/114.15.2), APC-Siglec-F (CD170, S17007L, BD bioscience). Post-acquisition analysis was performed using FlowJo software (TreeStar).

Blood samples were incubated on ice for 40 minutes in mouse CD16/CD32 hybridoma 2.4G2 supernatant to block IgG receptors and fluorescein isothiocyanate (FITC)-conjugated CD11b (M1/70) (101206, Biolegend), anti-CSF1R-PE-Cyanin7 (PECy7) (30-F11) (103149, BD Biosciences), Ly6G-APC-Cyanin7 (APCCy7) (1A8) (127624, BioLegend), and CD45-BV785 (103149, BD Biosciences) antibodies. Fixable viability stain (FVS)700 (564997, BD Bioscience) was added to all stained samples for dead cell exclusion. Samples were analysed on a Cytoflex (Beckman Coulter) flow cytometer equipped with 640nm, 561nm, 488nm, and 405nm lasers. Uncompensated FCS files were analysed using FlowJo10 software following compensation with single colour controls.

Histology

The left lobe of each mouse (both IAV and SARS-CoV-2) was inflated and fixed in 10% neutral buffered formalin for 24 h before being transferred to 70% ethanol for processing by the Core Histology Facility (Translational Research Institute, Australia). Paraffin-embedded samples were subsequently sectioned, deparaffinized and rehydrated before being stained with hematoxylin and eosin. Histopathological changes were scored by a pathologist blinded to the group treatments as previously described [6, 7].

Immunohistochemistry

Heat-induced epitope retrieval was performed using citrate buffer (pH 6, 95˚C, 30 mins) (BP327-1; Thermo Fisher Scientific). Sections were blocked for endogenous peroxidase activity using 3% hydrogen peroxide (HL001-2.5L-P, Chem Supply, Adelaide, South Australia), washed with tris-buffered saline (TBS; Bio-Rad) containing 0.05% polysorbate 20 (Tween-20; Sigma Aldrich; TBST) and blocked using background sniper (BS966, Biocare Medical, Concord, CA) for 30 mins. Immunolabelling was performed with rabbit antibodies against SARS-CoV-2 nucleocapsid protein antibody (1 hour at 25˚C, 1:5000) (40143-R040 Sino Biological), IBA1 (2 hours at 25˚C 1:1000) (019-19741; NovaChem), CH25H (4˚C overnight 1:600) (BS-6480R, Bioss Antibodies), CYP7B1 (4˚C overnight 1:1000) (BS-5052R, Bioss Antibodies), HSD3B7 (2 hours at 25˚C 1:600) (BS-2366R, Bioss Antibodies) and isotype control (rabbit IgG 31235, Thermo Fisher Scientific. Sections were washed with TBST and subsequently incubated with horseradish peroxidase (HRP)-conjugated goat anti-rabbit Ig antibody (1:200) (ab6721, Abcam) at 25˚C for 30 mins. Sections were washed with TBST before applying chromogen detection, using

diaminobenzidine (ab64238, DAB substrate kit Abcam,) as per the manufacturer's instructions. Counterstaining was performed with Mayer's hematoxylin (Sigma-Aldrich) before dehydrating the sections in a series of increasing ethanol concentrations (70% to 100% ethanol). Sections were clarified with xylene and mounted using a xylene-based mounting medium (15-184-40, SHURMount Mounting Media, Fisher scientific). Slides were scanned in an Olympus SLIDEVIEW VS200 using a 20x objective. DAB-positive areas were quantified using ImageJ (https://imagej.nih.gov/ij/) using a method previously described [8].

Mouse tissue sampling

At the endpoint of the experiments, mice were euthanised with CO2. The BM of one femur was flushed into 1 mL ice-cold phosphate buffered saline (PBS) containing 2% newborn calf serum (NCS) using a 1 mL syringe mounted with a 23G needle, and cells washed in this buffer for subsequent flow cytometry and colony assays. Blood was collected via cardiac puncture using a 1 mL syringe mounted with a 26G needle. Blood samples for flow cytometry were first cleaned by erythrocyte lysis by a 5-minute incubation in 5 volumes of 10 mM NaHCO3, 150 mM NH4Cl, 1 mM EDTA pH=7.4 buffer at room temperature. Blood leukocytes were then washed twice by centrifugation in PBS with 2% NCS. Blood samples were counted neat on Mindray BC-5000 Vet Auto hematology analyzer (Biomedical Electronics Co. LTD., China).

Bone marrow derived macrophage (BMDM) preparation and cell viability

BMDM were prepared by flushing the BM of 1 femur with PBS containing 2 % NCS. BM cells were washed with PBS and then diluted in 200µl RPMI-1640 supplemented

with 10% fetal calf serum (FCS, Life Technologies), 100ng/mL recombinant human macrophage colony-stimulating factor-1 (CSF1 was a kind gift from Prof David Hume, Mater Research), standard penicillin, gentamycin and glutamine and seeded in six 10 cm diameter Sterilin™ dishes (ThermoFisher Scientific, cat#SLN109) and 50,000 cells/well were cultured at 37ºC with 5% CO_2.

Colony forming assay

Bone marrow cell suspension aliquots corresponding to 1/1000 of a whole femoral marrow (in 10µL) were seeded in duplicate in 35 mm Petri dishes and covered with 1mL cytokine-free MethoCult medium (Cat# M3231, Stem Cell Technologies, Vancouver, Canada) supplemented with 100-ng/mL recombinant human CSF-1 (kindly donated by Prof David Hume). Colony forming units macrophage (CFU-M) were counted after 8 days of culture at 37 ºC in a 5% CO_2 humidified incubator.

***In vitro* infection/stimulation with IAV and LPS**

Bone marrow cells from the femur and tibia of 3 C57BL/6 and 3 *Gpr183-/-* mice were extracted as previously described [9]. 10 x 10^6 bone marrow cells were cultured in 10 ml of complete media (DMEM, 100 U/ml of penicillin-streptomycin and 10% FBS) in the presence of recombinant mouse macrophage colony-stimulating factor (mouse CSF-1; 50 ng/ml; Peprotech). On day 3, 10 ml of complete media containing 50 ng/ml CSF-1 was added. On day 6, adherent cells were collected as BMDMs. BMDMs were re-seeded to 24 well plates at a density of 3x10^5 cell/ml, left overnight in incubator before infection and/or stimulation. BMDMs are subsequently infected with A/Solomon Islands/03/06 at a multiplicity of infection (MOI) of 10, with or without 10µM NIBR189

for one hour. After one hour, cells were washed with DMEM containing 25mM HEPES (Thermofisher, 15630106) to remove excess viruses before media replacement containing NIBR189 for 24 hours. Cells were stimulated with LPS (100ng/mL) with or without 10μM NIBR189 for 24 hours. For RNA extraction, cells were lysed by adding 500 μL of TRIZol reagent.

Analysis of single cell RNA sequencing data

We accessed publicly available single cell RNA sequencing (scRNA-seq) data from nine COVID-19 patients (moderate: $n = 3$; severe: $n = 6$) and four healthy controls [10]. The dataset comprised a total of 66,452 cells from 32 cell type clusters, including eight major BALF immune cell types (i.e., macrophages, neutrophil, myeloid dendritic cells [mDCs], plasmacytoid dendritic cells [pDCs], T, NK, B, plasma), epithelial cells, and mast cells. We then tested for evidence of differential expression of four genes (*CH25H*, *CYP7B1*, *GPR183, HSD3B7*) between: (1) moderate COVID-19 cases and healthy controls; (2) severe COVID-19 cases and healthy controls; (3) COVID-19 cases and healthy controls; and (4) severe and moderate COVID-19 cases, for each major BALF cell type cluster and 16 macrophage sub-clusters. We estimated the average log fold change (logFC) per gene between groups using negative binomial generalised linear models applied to the raw unique molecular identifier (UMI) counts implemented in the Seurat software [11], and adjusted for covariates, including number of total UMI count per cell, number of genes detected per cell, and percent mitochondrial genes per cell. We also applied a non-parametric Wilcoxon rank sum test for normalised counts as a sensitivity analysis. We used Bonferroni correction to identify significant associations ($p < 1.30\times10^{-4}$; i.e.,

$\frac{0.05}{24\ clusters \times 4\ genes \times 4\ comparisons}$) and further required that genes be expressed in at least 5% of cells in both groups with an absolute value of average log fold change (logFC) greater than 0.25.

Supplementary figures

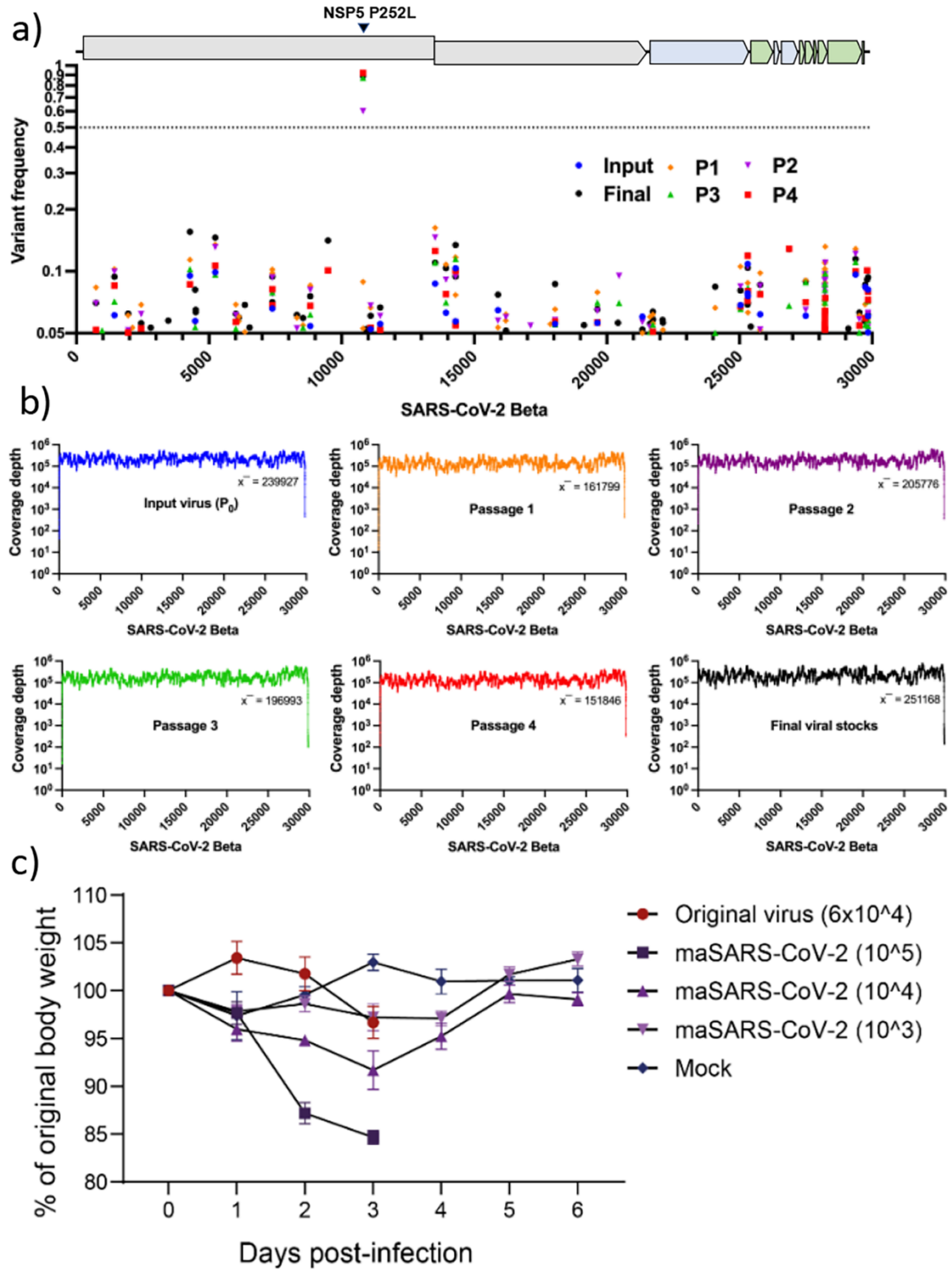

Figure S1. Evolution and coverage of mouse-adapted SARS-CoV-2 virus. a) Mutation frequency of input SARS-CoV-2 Beta virus (blue circle) and passage one (orange diamond), passage two (purple nabla), passage three (green triangle) and

passage four (red square) mouse-adapted viruses over the reference genome sequence as well as the final virus stocks (black circle) amplified in VeroE6-hTMPRSS2 cells. The dotted line indicates the consensus frequency of 0.5 b) Summary plots of read coverage of passaged SARS-CoV-2 viruses from a) mapping to SARS-CoV-2 Beta strain. Depth of coverage of binary alignment files was determined using samtools depth. c) Weight loss over time following infection with the Beta variant of SARS-CoV-2 (original virus) or various doses of maSARS-CoV-2 (after four passages in mice). Plaque forming units are indicated in brackets. Data indicates mean ± SEM.

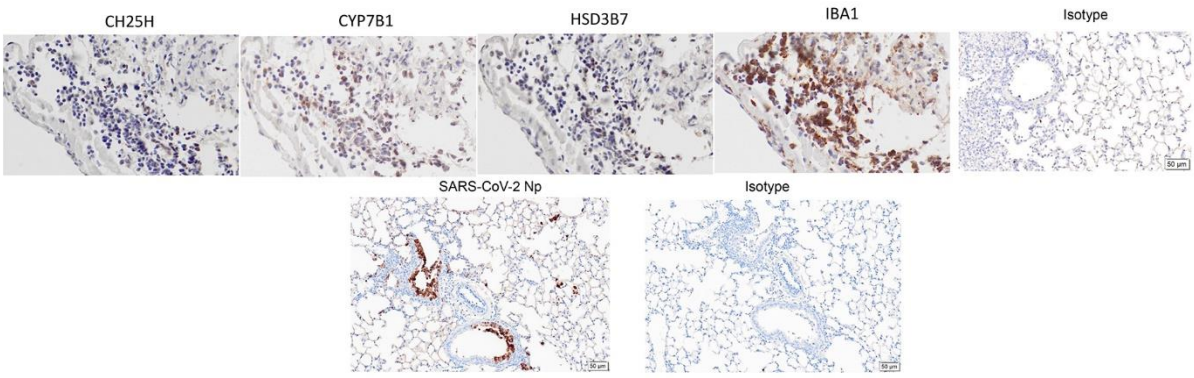

Figure S2. Isotype staining controls for CYP7B1, CH25H, IBA1 and viral Np. IHC of IAV-infected lung sections incubated with rabbit anti-CH25H, rabbit anti-CYP7B, rabbit anti-HSD3B7, rabbit anti-IBA1 and an isotype-matched control (Rabbit IgG; negative control). IHC of SARS-CoV-2-infected lung sections incubated with rabbit anti-SARS-CoV-2 nucleocapsid protein (Np) and an isotype-matched control (Rabbit IgG; negative control). Scale bar = 50μm

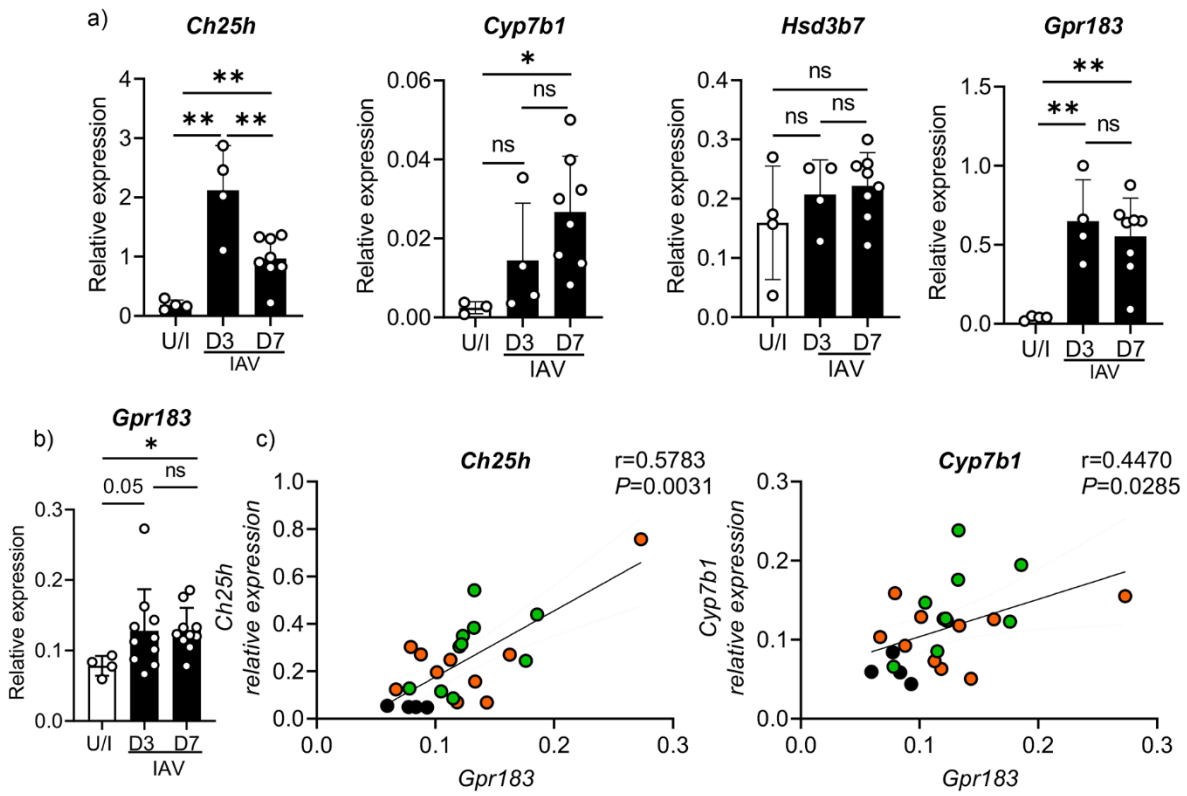

Figure S3. *Ch25h, Cyp7b1, Hsd3b7* and *Gpr183* mRNA expression is upregulated in the BAL cells during IAV infection and *Gpr183* expression in the lung tissue correlates with expression of the oxysterol synthesising enzymes CH25H and CYP7B1. C57BL/6J mice were infected intranasally with 5,500 PFU of IAV. Relative expression of *Ch25h*, *Cyp7b1*, *Hsd3b7* and *Gpr183* mRNA measured by RT-qPCR, normalised to *Hprt from a) BAL cell pellet and b) lung tissue*. Correlation analyses were performed with mRNA expression levels of *Gpr183* and oxysterol synthesising enzymes from lung tissue. Individual scatter plots showing correlations between *Gpr183* and *Ch25h* and *Cyp7b1*. Black dots represent uninfected samples while coloured dots represent IAV-infected samples (Orange dots, 3 dpi; green dots, 7 dpi). Data are presented as mean ± SD of n=4 uninfected and n=8-10 infected mice per timepoint. ns = not significant; *, $P < 0.05$; **, $P < 0.01$ indicate significant differences. Spearman rank correlation test were used to calculate the correlation coefficient and to determine significant correlations with values displayed on each scatter plot.

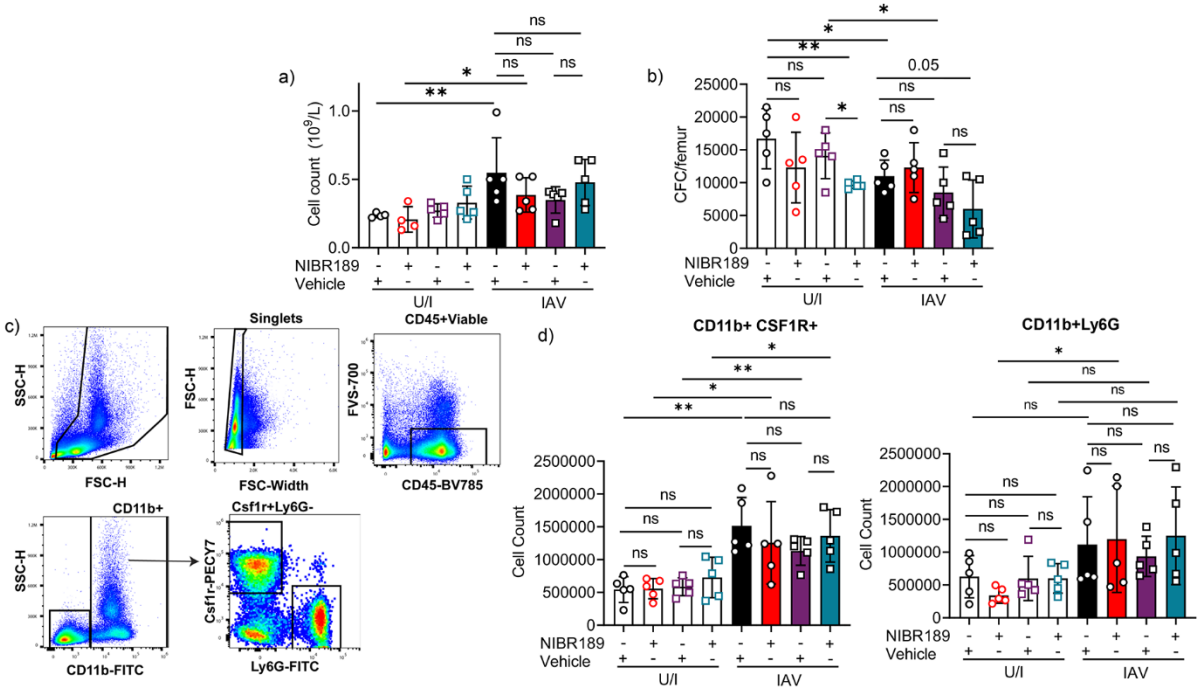

Figure S4. C57BL/6J or *Gpr183*$^{-/-}$ mice were infected intranasally with 5,500 PFU of IAV or mock infected (U/I). Mice were subsequently treated orally with 7.6 mg/kg NIBR189 or vehicle control twice daily from 1 dpi until the end of the experiment. a) blood monocyte cell counts on differential blood analyser b) bone marrow CFU-M numbers per femur in colony forming assays with recombinant CSF-1, c) gating strategy and d) cell counts (cells per mL blood) of CD45$^+$ CD11b$^+$ CSF1R$^+$ Ly6G$^-$ monocytes and CD45$^+$ CD11b$^+$ CSF1R$^-$ Ly6G$^+$ neutrophils by flow cytometry.

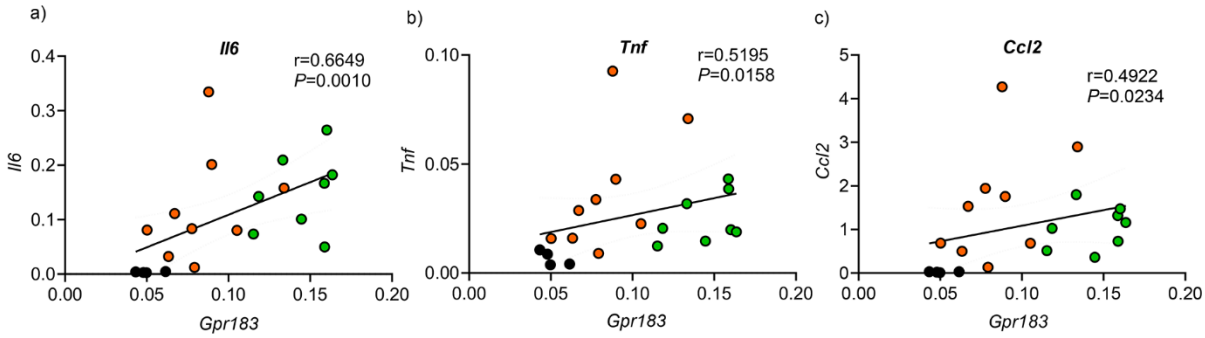

Figure S5. **Correlations between lung mRNA expression of *Gpr183* and inflammatory markers in IAV-infected mice.**

Correlation analyses of *Gpr183* mRNA expression with mRNA expression of inflammatory cytokines in lung tissue from IAV-infected C57BL/6J mice (n=21 pairs). Relative gene expression was determined by RT-qPCR, normalised to *Hprt*. Individual scatter plots showing correlations between *Gpr183* and a) *Il6*, b) *Tnf* and c) *Ccl2*. Black dots represent uninfected samples while coloured dots represent IAV-infected samples (orange dots, 3dpi; green dots, 7dpi). Spearman rank correlation tests were used to calculate correlation coefficient and to determine significant correlations with values displayed on each scatter plot.

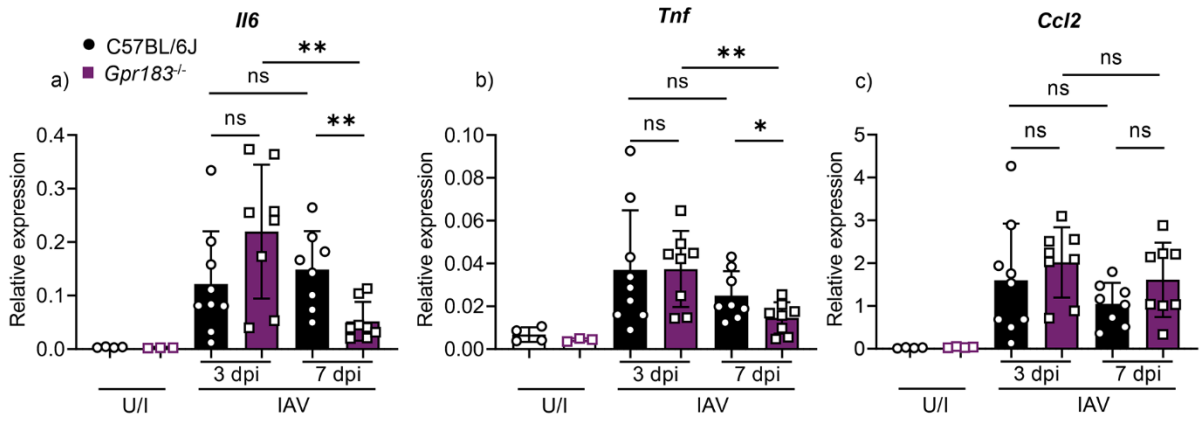

Figure S6. Cytokine expression at mRNA and protein level in IAV-infected C57BL/6J and *Gpr183*$^{-/-}$ mice. C57BL/6J and *Gpr183*$^{-/-}$ mice were infected intranasally with 5,500 PFU of IAV. Cytokine measurements of a) *Il6,* b) *Tnf* and c) *Ccl2* at 3 dpi and 7 dpi measured by RT-qPCR, normalised to *Hprt.* Data are presented as mean ± SD of n=4 uninfected per genotype and n=8-10 infected mice per genotype and timepoint. U/I = uninfected; dpi = days post-infection; ns = not significant; *, $P < 0.05$; **, $P < 0.01$ indicate significant differences.

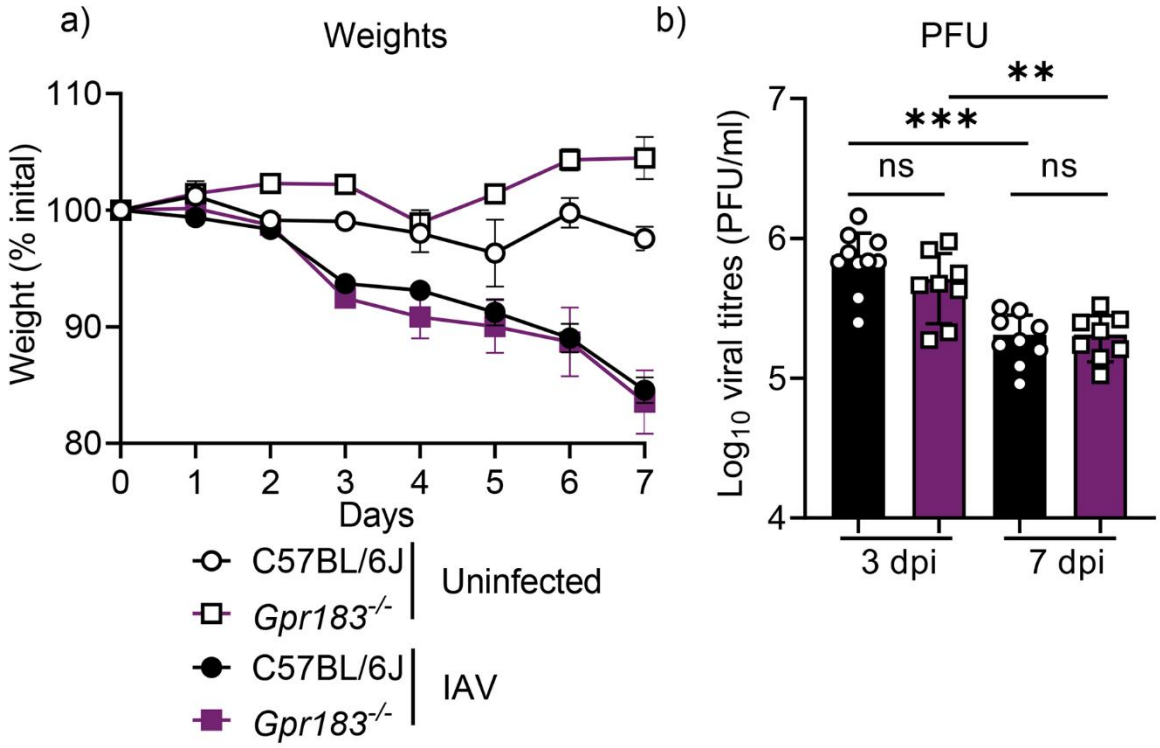

Figure S7. Weights of IAV and mock infected C57BL/6J and *Gpr183*$^{-/-}$ mice and viral loads. C57BL/6J and *Gpr183*$^{-/-}$ mice were infected intranasally with approximately 5,500 PFU of IAV. a) Weights of IAV- or uninfected, mock-inoculated mice are displayed as percentage of the weight at time of inoculation. b) Viral loads were assessed by measuring the PFU by plaque assays. Data are presented as mean ± SD for n=8-10 infected mice per genotype and timepoint. dpi = days post-infection; ns = not significant; **, $P < 0.01$; ***, $P < 0.001$ indicate significant differences.

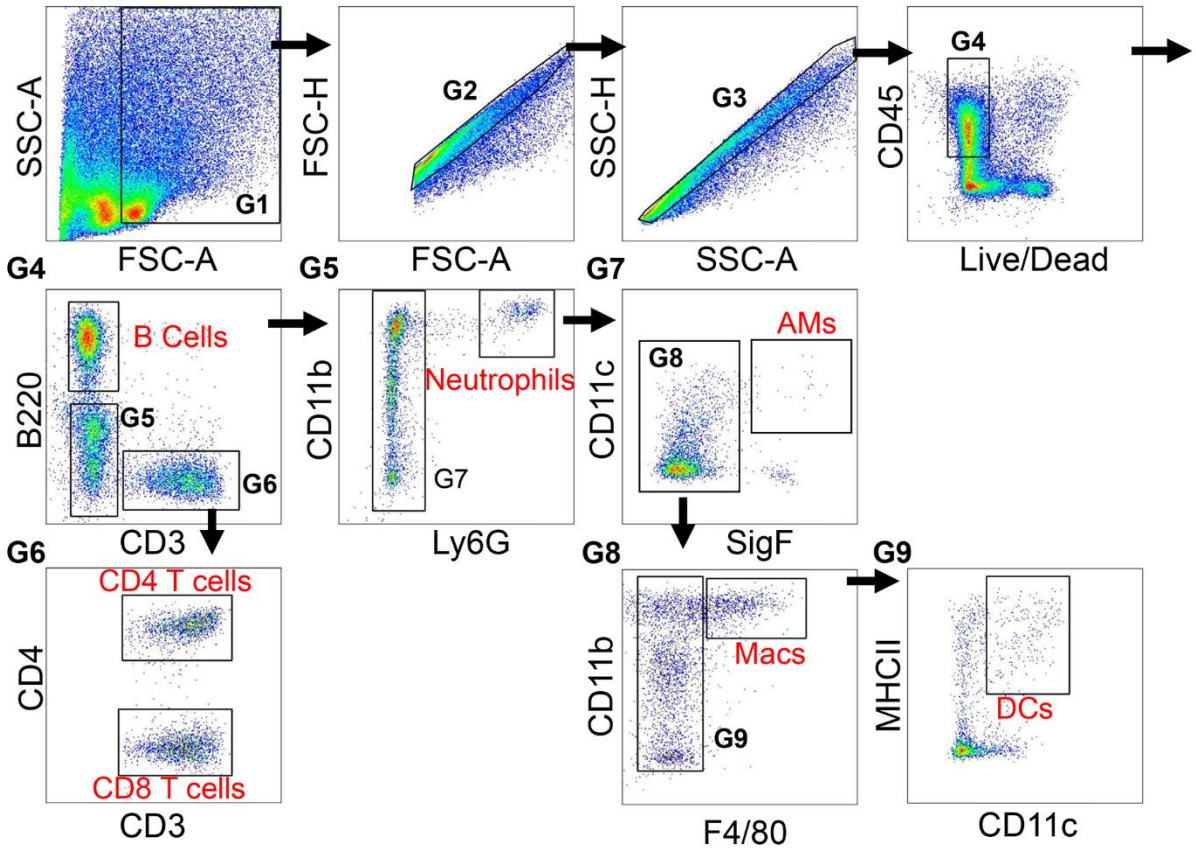

Figure S8. Representative flow cytometry plots illustrating the gating strategy for immune cells in lung single cells suspension. Gates containing multiple cell populations are numbered (G1-G9). Gates that contained a single cell population are labeled with its respective cell type. These includes: B cells ($B220^+$; G5), $CD4^+$ T cells ($CD3^+$,$CD4^+$; G6), $CD8^+$ T Cells ($CD3^+$,$CD4^-$; G6), Neutrophils ($B220^-$,$CD3^-$,$Ly6G^+$; G5), Alveolar macrophages ($B220^-$,$CD3^-$,$Ly6G^-$,$CD11c^+$,$SigF^+$; G7), Macrophages ($B220^-$,$CD3^-$,$Ly6G^-$,$SigF^-$,$CD11b^+$,$F4/80^{high}$; G8) and Dendritic cells (DCs; $B220^-$,$CD3^-$,$Ly6G^-$,$SigF^-$, $F4/80^{low}$,$CD11c^+$, $MHCII^+$; G9).

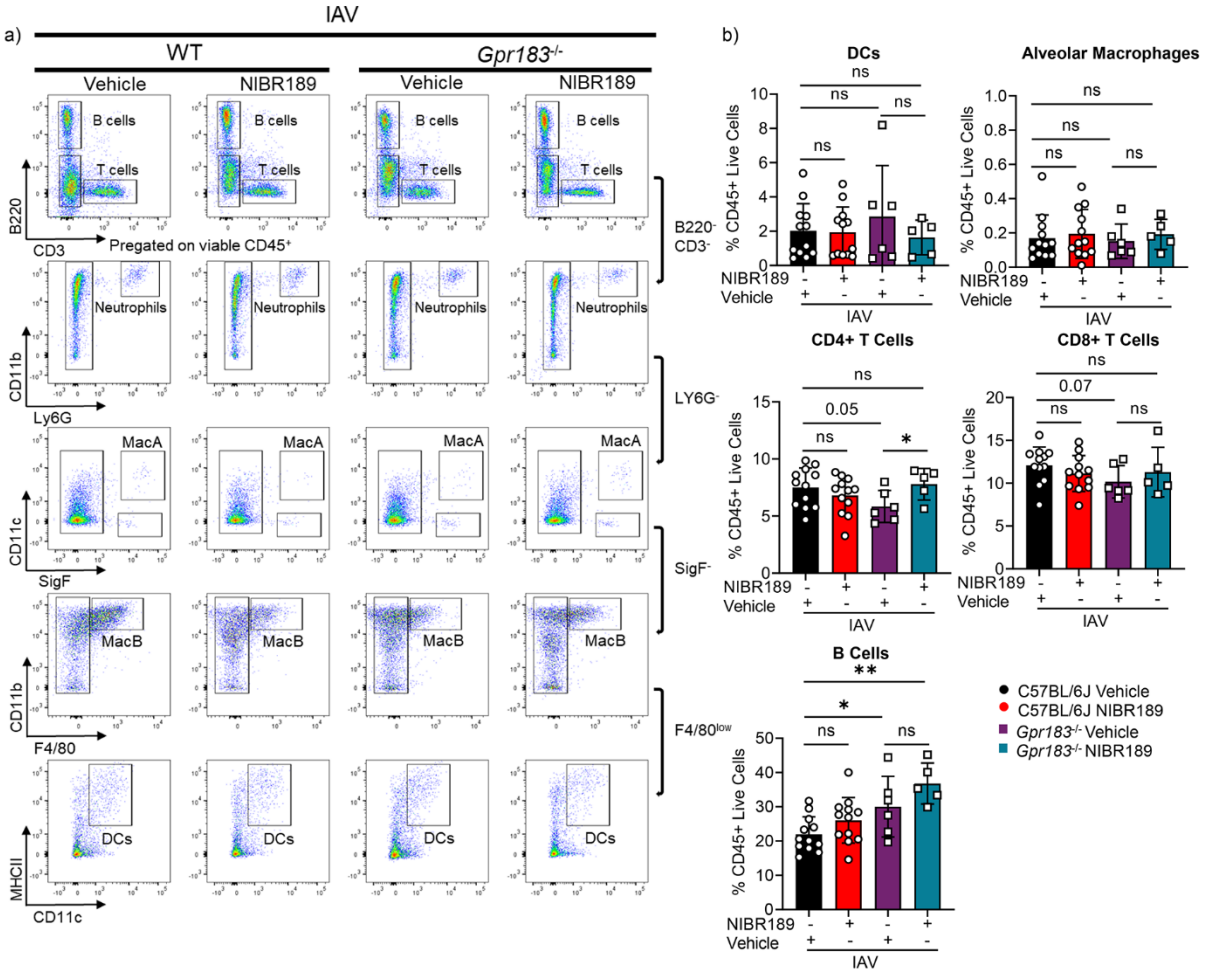

Figure S9. Immune cell populations in the lungs of IAV-infected mice treated with the GPR183 antagonist NIBR189. C57BL/6J or *Gpr183*$^{-/-}$ mice were infected intranasally with 5,500 PFU of IAV. Mice were subsequently treated orally with 7.6 mg/kg NIBR189 or vehicle control twice daily from 1 dpi until the end of the experiment. a) Frequencies of B cells (B220^{+}), T cells (CD3^{+} CD8^{+} or CD4^{+}), neutrophils (B220^{-} CD3^{-}Ly6G^{+}) were determined by flow cytometry against total viable CD45^{+} immune cells at 3 dpi. Alveolar macrophages (CD11c^{+}SigF^{+}), infiltrating macrophages (F480^{high}/CD11b^{+}/Ly6G^{-}/SigF^{-}) and dendritic cells (SigF^{-}F4/80^{-}MHCII^{+}CD11c^{+}) were further identified from the B220^{-}CD3^{-}Ly6G^{-} cell population. B) Graphs depicting the frequency of Dendritic cells, alveolar macrophages, CD4^{+} T cells, CD8^{+} T cells and B cells against total viable CD45^{+} immune cells. Data are presented mean ± SD of n=5-

12 infected mice per genotype and timepoint. UI = uninfected; dpi = days post-infection; ns = not significant.

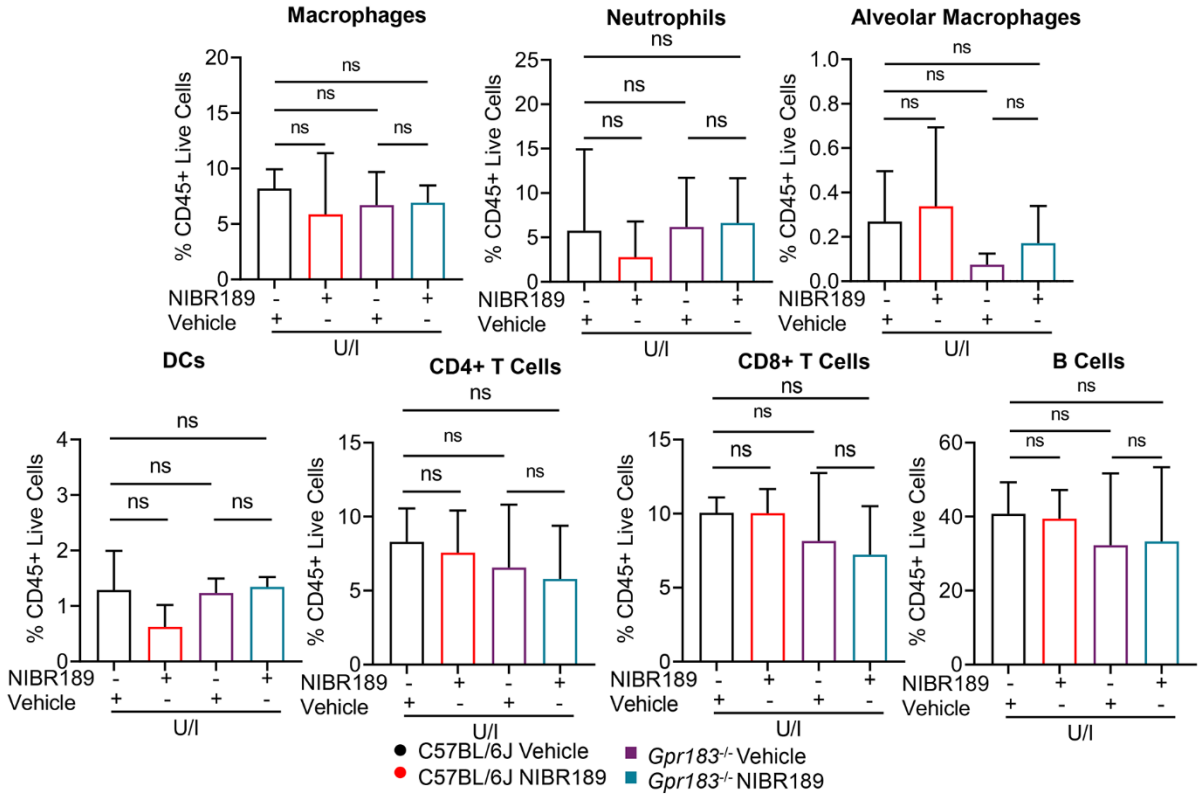

Figure S10. Immune cell populations in the lungs of uninfected mice treated with the GPR183 antagonist NIBR189. C57BL/6J or *Gpr183*$^{-/-}$ mice were mock infected intranasally with PBS. Mice were subsequently treated orally with 7.6 mg/kg NIBR189 or vehicle control twice daily from 1 dpi until the end of the experiment. Graphs show the frequencies of macrophages, neutrophils, alveolar macrophages, B cells CD4^{+} T cells, CD8^{+} T cells and Dendritic cells against total viable CD45^{+} immune cells at 3 dpi. Data are presented mean ± SD of n=2-3 uninfected mice per genotype and timepoint. UI = uninfected; ns = not significant.

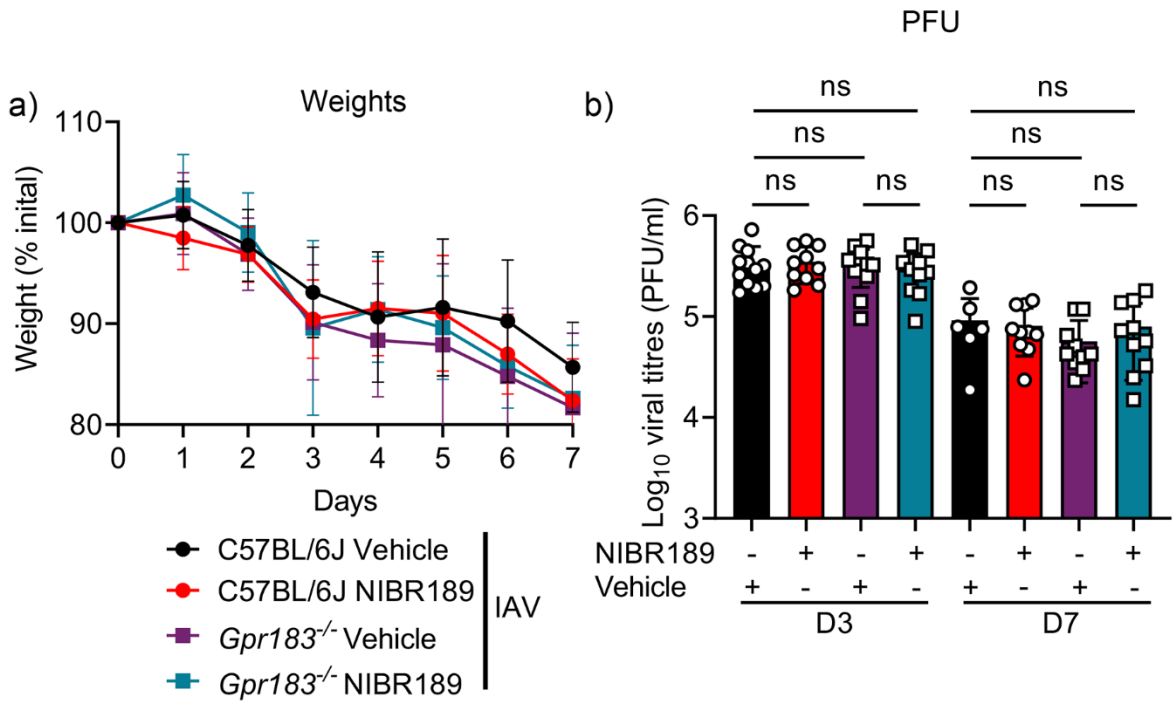

Figure S11. Body weights and viral loads of IAV-infected C57BL/6J and *Gpr183*$^{-/-}$ mice treated with NIBR189 or vehicle. C57BL/6J mice and *Gpr183*$^{-/-}$ mice were infected intranasally with 5,500 PFU of IAV. Mice were subsequently treated orally with 7.6 mg/kg NIBR189 or vehicle control twice daily from 1 dpi until the end of the experiment. a) Weights of IAV- or mock-inoculated mice with or without treatment are displayed as percentage of the weight at time of inoculation. b) Viral loads were assessed by measuring the PFU by plaque assay. Data are presented as mean ± SEM or SD of n=6-12 infected mice per genotype and timepoint. UI = uninfected; dpi = days post-infection; ns = not significant.

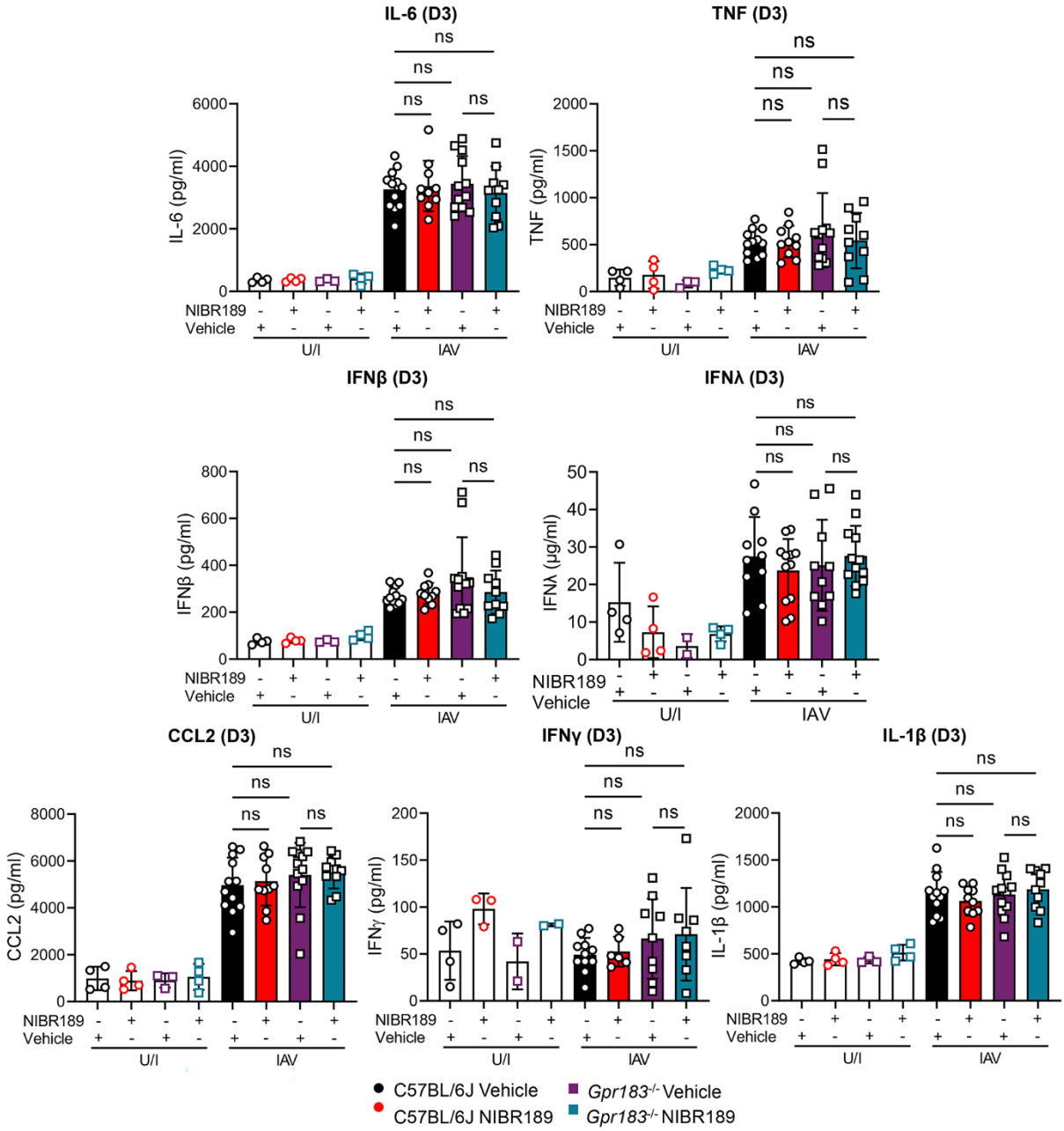

Figure S12. Cytokine concentrations in IAV-infected C57BL/6J and *Gpr183*$^{-/-}$ mice treated with NIBR189 and/or vehicle. C57BL/6J and *Gpr183*$^{-/-}$ mice were infected intranasally with 5,500 PFU of IAV. Mice were subsequently treated orally with 7.6 mg/kg NIBR189 or vehicle control twice daily from 1 dpi until the end of the experiment. Cytokine measurements of IL-6 TNF, IFNβ, IFN*λ*, CCL2 IFNγ and IL-1β, at 3 dpi measured by ELISA. Data are presented as mean ± SD of n=4 uninfected mice

per genotype and n=6-12 infected mice per genotype. U/I = uninfected; dpi = days post-infection; ns = not significant. *, $P < 0.05$ indicate significant differences.

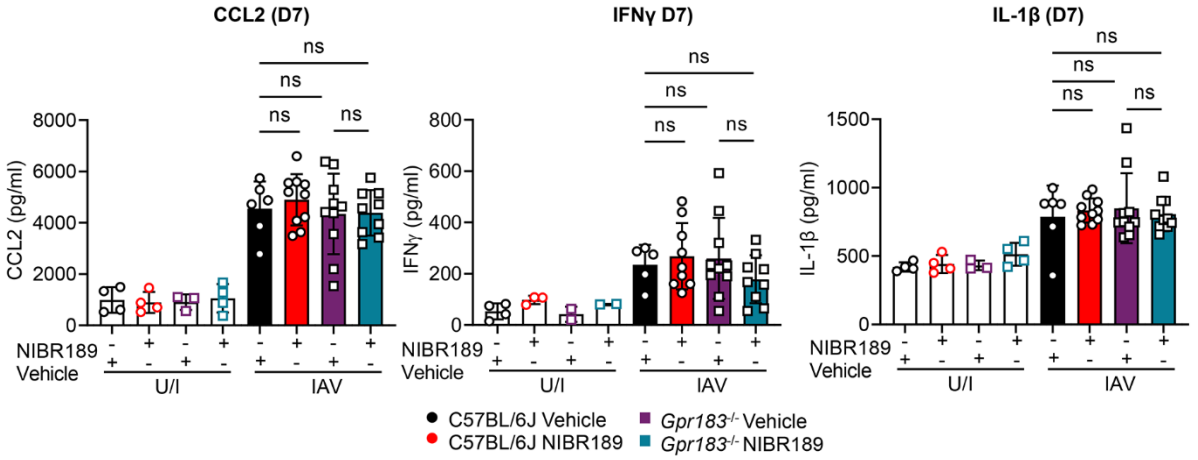

Figure S13. Cytokine concentrations in IAV-infected C57BL/6J and *Gpr183*$^{-/-}$ mice treated with NIBR189 and/or vehicle. C57BL/6J and *Gpr183*$^{-/-}$ mice were infected intranasally with 5,500 PFU of IAV. Mice were subsequently treated orally with 7.6 mg/kg NIBR189 or vehicle control twice daily from 1 dpi until the end of the experiment. Cytokine concentrations of CCL2, IFNγ, and IL-1β at 7 dpi were measured by ELISA. Data are presented as mean ± SD of n=4 uninfected mice per genotype and n=6-12 infected mice per genotype. U/I = uninfected; dpi = days post-infection; ns = not significant.

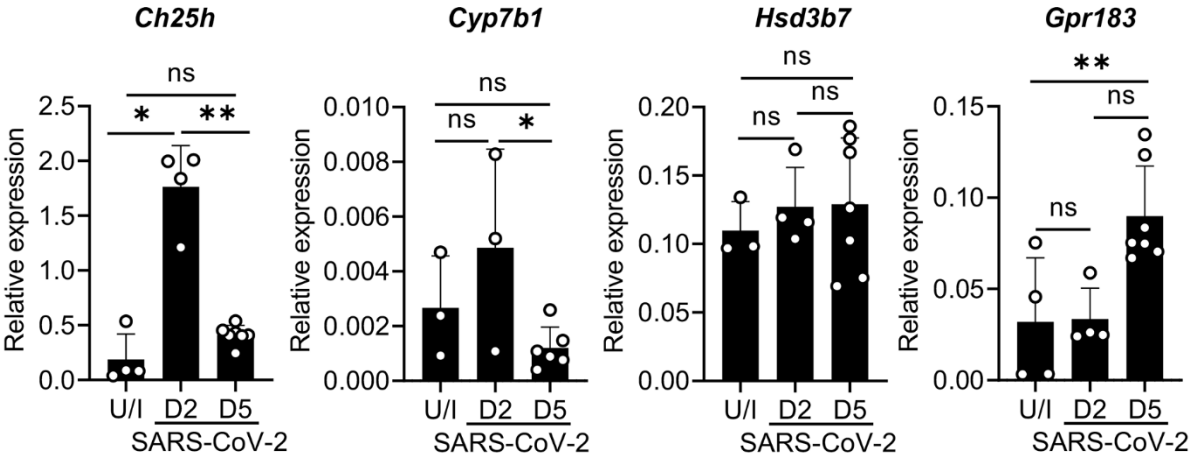

Figure S14. *Gpr183, Ch25h, Cyp7b1* and *Hsd3b7* mRNA expression in BALF during SARS-CoV-2 infection. C57BL/6J and *Gpr183*$^{-/-}$ mice were infected intranasally with approximately 8x10^4 PFU of mouse-adapted SARS-CoV-2. Relative expression of *Gpr183*, *Ch25h*, *Cyp7b1*, *Hsd3b7* and *Gpr183* mRNA measured by RT-qPCR, normalised to *Hprt in BAL cells*. Data are presented as mean ± SD of n=3-4 uninfected and n=4-7 infected mice per timepoint. ns = not significant; *, $P < 0.05$; **, $P < 0.01$ indicate significant differences.

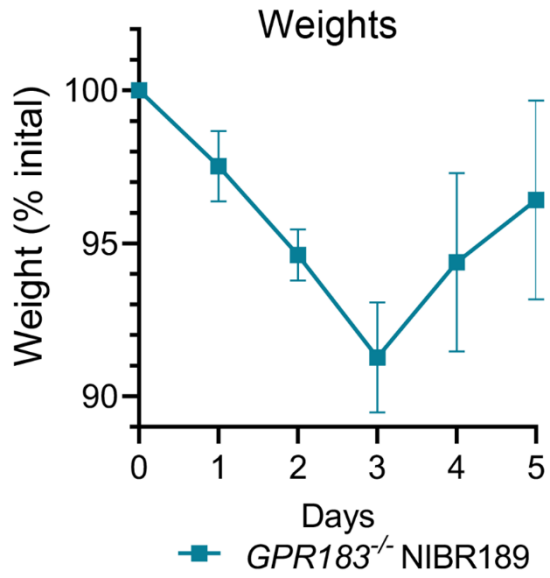

Figure S15. Body weights of *Gpr183-/-* mice upon SARS-CoV-2 infection. *Gpr183*$^{-/-}$ mice were infected intranasally with approximately 8x10^4 PFU of mouse-adapted SARS-CoV-2. Mice were subsequently treated orally with 7.6 mg/kg NIBR189 or vehicle control twice daily from 1 dpi until the end of the experiment. Weights of mice displayed as percentage of the weight at time of inoculation. Data are presented as mean ± SEM, n=10.

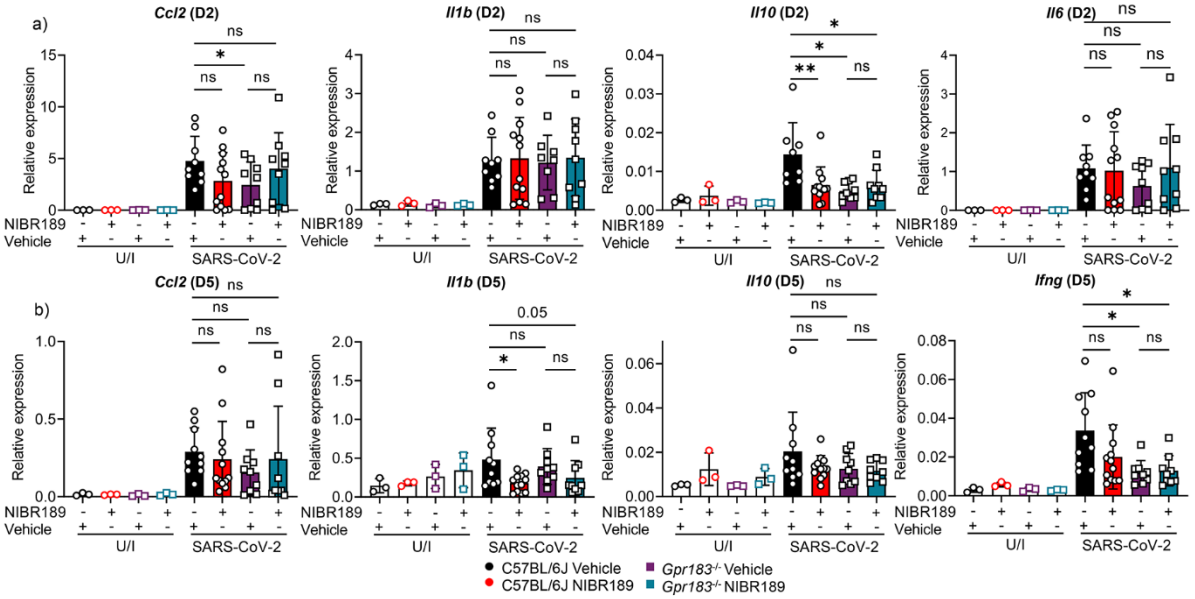

Figure S16. Cytokine mRNA expression in SARS-CoV-2-infected C57BL/6J and *Gpr183*$^{-/-}$ mice treated with GPR183 antagonist at 2 dpi and 5 dpi. C57BL/6J and *Gpr183*$^{-/-}$ mice were infected intranasally with approximately 8x10^4 PFU of mouse-adapted SARS-CoV-2. Mice were subsequently treated orally with 7.6 mg/kg NIBR189 or vehicle control twice daily from 1 dpi until the end of the experiment. Expression of a) *Ccl2*, *Il1b Il10* and *Il6* at 2 dpi and b) *Ccl2*, *Il1b, Il10* and *Ifng* 5 dpi was measured by RT-qPCR normalised to *Hprt*. Data are presented as mean ± SD of n=3 uninfected mice and n= 9-12 infected; mice per genotype and timepoint. U/I = uninfected dpi = days post-infection; ns = not significant. *, $P < 0.05$; **, $P < 0.01$; ***, $P < 0.001$ indicate significant differences.

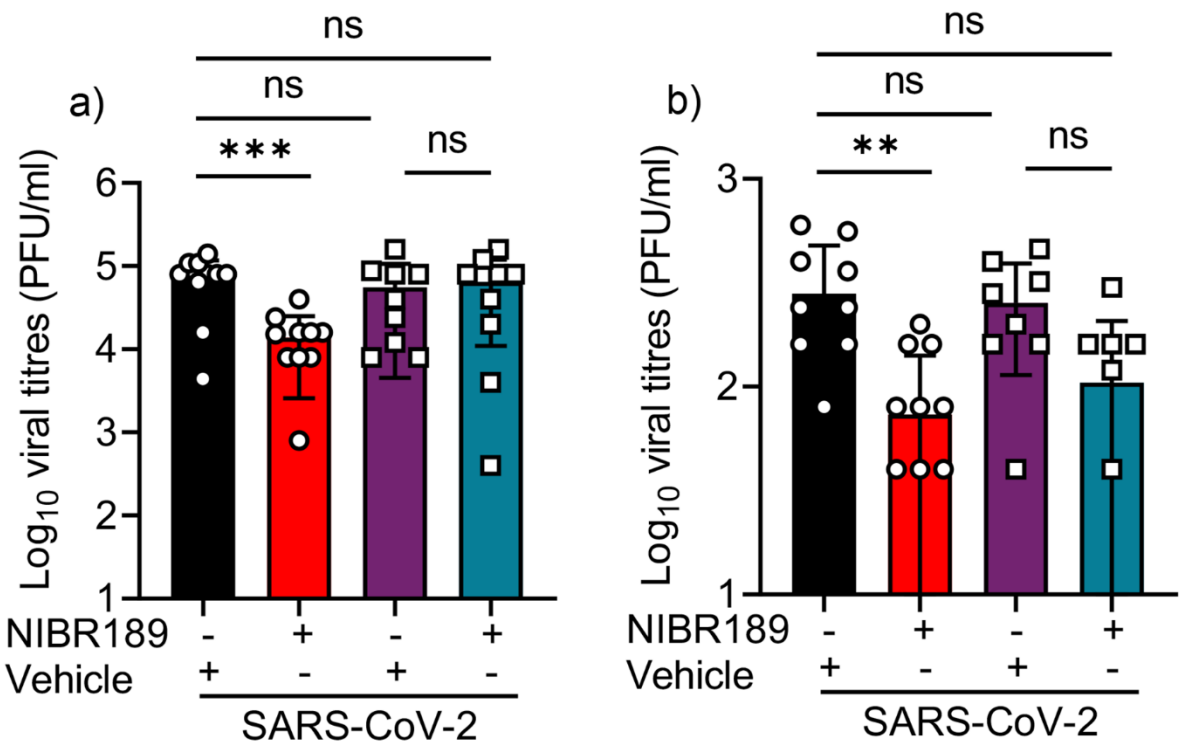

Figure S17. Viral loads of SARS-CoV-2-infected C57BL/6J and *Gpr183*$^{-/-}$ mice treated with NIBR189 or vehicle. C57BL/6J and *Gpr183*$^{-/-}$ mice were infected intranasally with approximately 8x10^4 PFU of mouse-adapted SARS-CoV-2. Mice were subsequently treated orally with 7.6 mg/kg NIBR189 or vehicle control twice daily from 1 dpi until the end of the experiment. Viral loads were assessed by measuring the PFU through plaque assay. Data are presented as mean ± SEM or SD of n=6-12 infected mice per genotype and timepoint. UI = uninfected; dpi = days post-infection; ns = not significant. ns = not significant. *, $P < 0.05$; **, $P < 0.01$; ***, $P < 0.001$ indicate significant differences.

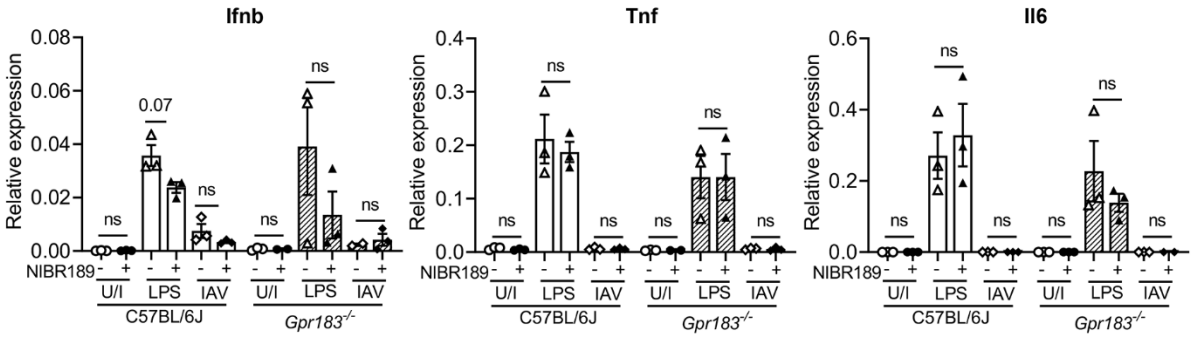

Figure S18. Cytokine mRNA expression in IAV-infected BMDMs from C57BL/6J and *Gpr183*$^{-/-}$ mice treated with GPR183 antagonist. BMDMs were infected with A/Solomon Islands/03/06 at a multiplicity of infection (MOI) of 10, with or without 10µM NIBR189 for one hour. After one hour, cells were washed to remove excess viruses before media replacement containing NIBR189 for 24 hours. Cells were stimulated with LPS (100 ng/mL) with or without 10µM NIBR189 for 24 hours, thereafter mRNA expression of *tnf*, *il6* or *ifnb* was determined by RT-qPCR normalised to *Hprt.*

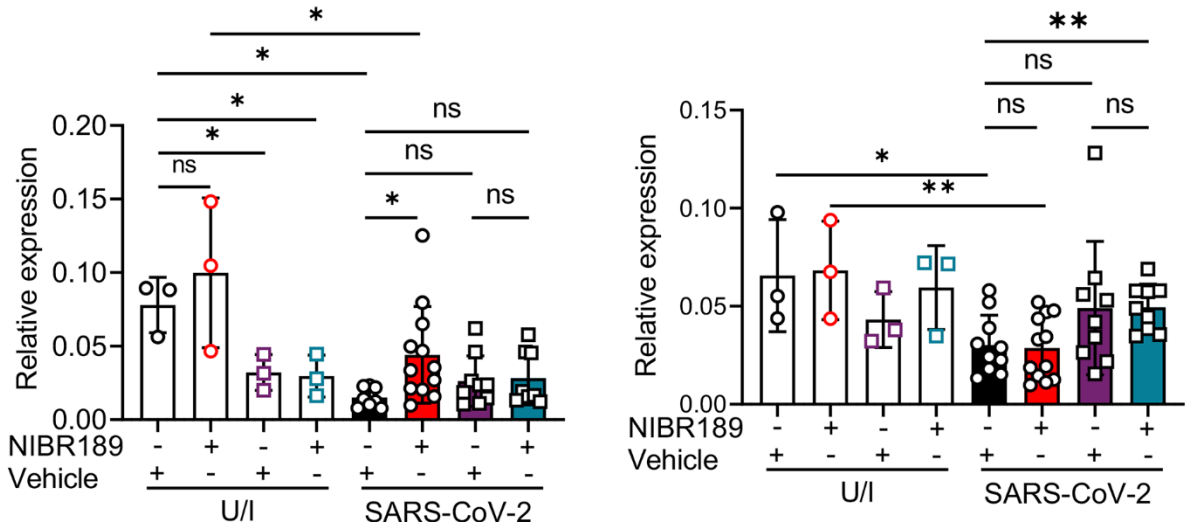

Figure S19. *Ace2* mRNA expression in the lung during SARS-CoV-2 infection. C57BL/6J and *Gpr183*$^{-/-}$ mice were infected intranasally with approximately 8x10^4 PFU of mouse-adapted SARS-CoV-2. Relative expression of *Ace2* mRNA was measured by RT-qPCR, normalised to *Hprt* in lung tissue. Data are presented as mean ± SD of

n=3-4 uninfected and n=4-7 infected mice per timepoint. ns = not significant; *, $P < 0.05$; **, $P < 0.01$ indicate significant differences.

Supplemental Table S1: Primers used in this study

	Forward	Reverse
Gpr183	GTCGTGTTCATCCTGTGCTTCAC	TCATCAGGCACACCGTGAAGTG
Ch25h	CTGACCTTCTTCGACGTGCT	GGGAAGTCATAGCCCGAGTG
Cyp7b1	CGGAAATCTTCGATGCTCCAAAG	GCTTGTTCCGAGTCCAAAAGGC
Hsd3b7	ACTGCGCTTTGGAGGTCGTCTA	GCCACCAGTATGTGCATCCAAG
Ccl2	GCTACAAGAGGATCACCAGCAG	GTCTGGACCCATTCCTTCTTGG
Hprt1	CCCCAAAATGGTTAAGGTTGC	AACAAAGTCTGGCCTGTATCC
Ifnb1	AACTCCACCAGCAGACAGTG	GGTACCTTTGCACCCTCCAG
Ifng	CAGCAACAGCAAGGCGAAAAAGG	TTTCCGCTTCCTGAGGCTGGAT
Il10	CGGGAAGACAATAACTGCACCC	CGGTTAGCAGTATGTTGTCCAGC
Il1b	TGGACCTTCCAGGATGAGGACA	GTTCATCTCGGAGCCTGTAGTG
Il6	CTGCAAGTGCATCATCGTTGTTC	TACCACTTCACAAGTCGGAGGC
Ifnl	AGCTGCAGGCCTTCAAAAAG	TGGGAGTGAATGTGGCTCAG
Tnf	TAGCCCACGTCGTAGCAAAC	ACAAGGTACAACCCATCGGC
mpro	GAGACAGGTGGTTTCTCAATCG	ACGGCAATTCCAGTTTGAGC
Ace2	TCCATTGGTCTTCTGCCATCC	AACGATCTCCCGCTTCATCTC

References

1. Langmead B, Salzberg SL. Fast gapped-read alignment with Bowtie 2. Nat Methods 2012: 9(4): 357-359.

2. Grubaugh ND, Ladner JT, Lemey P, et al. Tracking virus outbreaks in the twenty-first century. Nat Microbiol 2019: 4(1): 10-19.

3. Thorvaldsdottir H, Robinson JT, Mesirov JP. Integrative Genomics Viewer (IGV): high-performance genomics data visualization and exploration. Brief Bioinform 2013: 14(2): 178-192.

4. Short KR, Diavatopoulos DA, Reading PC, et al. Using bioluminescent imaging to investigate synergism between Streptococcus pneumoniae and influenza A virus in infant mice. J Vis Exp 2011(50).

5. Schimmel L, Chew KY, Stocks CJ, et al. Endothelial cells are not productively infected by SARS-CoV-2. Clin Transl Immunology 2021: 10(10): e1350.

6. McMillan CLD, Choo JJY, Idris A, et al. Complete protection by a single-dose skin patch-delivered SARS-CoV-2 spike vaccine. Sci Adv 2021; 7: eabj8065.

7. Marshall RJ, Armart P, Hulme KD, et al. Glycemic Variability in Diabetes Increases the Severity of Influenza. mBio 2020; 11: e02841-19.

8. Crowe AR, Yue W. Semi-quantitative Determination of Protein Expression using Immunohistochemistry Staining and Analysis: An Integrated Protocol. Bio Protoc 2019; 9: e3465.

9. Liu X, Quan N. Immune Cell Isolation from Mouse Femur Bone Marrow. Bio Protoc 2015: 5(20).

10. Liao M, Liu Y, Yuan J, et al. Single-cell landscape of bronchoalveolar immune cells in patients with COVID-19. Nat Med 2020: 26(6): 842-844.

11. Hao Y, Hao S, Andersen-Nissen E, et al. Integrated analysis of multimodal single-cell data. Cell 2021: 184(13): 3573-3587 e3529.